Transcriptomic profiling of autophagy and apoptosis pathways in liver cancer cells treated with a new tyrosine kinase inhibitor PD161570

XINGXING HE[1*], JIANPING LIU[1*], YULIAN ZHANG[2,3] and BUSHAN XIE[1-3]

[1]Department of Gastroenterology, Digestive Disease Hospital, The First Affiliated Hospital, Jiangxi Medical College, Nanchang University, Nanchang, Jiangxi 330006, P.R. China; [2]Jiangxi Provincial Key Laboratory of Digestive Diseases, The First Affiliated Hospital, Jiangxi Medical College, Nanchang University, Nanchang, Jiangxi 330006, P.R. China; [3]Jiangxi Clinical Research Center for Gastroenterology, The First Affiliated Hospital, Jiangxi Medical College, Nanchang University, Nanchang, Jiangxi 330006, P.R. China

Received June 10, 2024; Accepted February 10, 2025

DOI: 10.3892/mmr.2025.13540

Abstract. Liver cancer is the third most lethal and prevalent cancer in the Asia-Pacific regions. Despite the use of tyrosine kinase inhibitors as first- and second-line therapies, the overall survival rate for advanced liver cancer remains dismal and has not improved over the past decade. The present study, through high-throughput screening, identified and demonstrated that PD161570, a new tyrosine kinase inhibitor, inhibited cell growth and proliferation in liver cancer cells. Mechanistically, PD161570 induced autophagy and enhanced autophagic flux in an autophagy-related gene (ATG5)-dependent and mammalian target of rapamycin kinase-independent manner. Furthermore, when combined with chloroquine treatment, PD161570 not only suppressed cell proliferation but also increased cell apoptosis due to autophagy inhibition. RNA sequencing analysis revealed 1,121 differentially expressed genes in liver cancer cells following PD161570 treatment under autophagy inhibition via ATG5 knockdown. Notably, key molecules involved in autophagy (such as Damage Regulated Autophagy Modulator 1) and apoptosis regulators (including HRK, CTSS, BIRC3, BBC3, DDIT3 and GADD45B), were identified. Functional enrichment analyses, including Gene Ontology (GO) and Kyoto Encyclopedia of Genes and Genomes (KEGG), demonstrated enrichment in apoptotic and cell death signaling pathways, highlighting the critical role of the mitogen-activated protein kinases signaling pathway. In conclusion, PD161570 elicited an ATG5-dependent autophagic process in liver cancer cells, while simultaneously enhancing apoptosis under conditions of autophagy inhibition.

Introduction

Liver cancer ranks as the third most prevalent cause of tumor-related mortality in the Asia-Pacific regions, with over half of the cases originating in China (1). Individuals with advanced liver cancer typically undergo various systemic treatment modalities (2). Over recent decades, remarkable strides have been made in managing intermediate and advanced-stage liver cancer, primarily due to advancements in targeted chemotherapy and immunotherapy (3). These breakthroughs have markedly improved overall survival rates and the quality of life for affected individuals. The majority of FDA-approved drugs for liver cancer are tyrosine kinase inhibitors (TKIs), such as sorafenib, lenvatinib, regorafenib, cabozantinib and ramucirumab (4). This preference is due to the pivotal role of tyrosine kinases in governing diverse biological processes such as growth, differentiation, adhesion, motility, metabolism and apoptosis in both normal and cancer cells (5,6). However, a significant drawback of TKIs is their propensity for acquired resistance (7,8), underscoring the critical need for novel-generation TKIs to provide second and third-line therapeutic options for patients with liver cancer.

In the present study, the TKI lead compound PD161570, a fibroblast growth factor receptor inhibitor, demonstrated a dose- and time-dependent inhibition of liver cancer cell viability. Subsequent investigations showed that PD161570 induced autophagy-related gene (ATG5)-dependent autophagic flux in hepatoma cells. RNA sequencing (RNA-seq) analyses and subsequent validation experiments confirmed PD161570's ability to initiate apoptotic cell death through pathway under conditions of autophagy inhibition. These findings underscore the importance of further investigations to assess the potential of this novel TKI as a therapeutic agent for liver cancer treatment.

Correspondence to: Dr Bushan Xie, Department of Gastroenterology, Digestive Disease Hospital, The First Affiliated Hospital, Jiangxi Medical College, Nanchang University, 18 Yong Wai Zheng Street, Nanchang, Jiangxi 330006, P.R. China
E-mail: 2267582610@qq.com

*Contributed equally

Key words: liver cancer, PD161570, autophagy, apoptosis, tyrosine kinase inhibitor

Materials and methods

Antibodies and reagents. PD161570 and chloroquine (CQ; cat. no. C6628) were acquired from MilliporeSigma. The antibody against p62 (cat. no. PA5-20839) was supplied by Invitrogen (Thermo Fisher Scientific, Inc.). Antibodies for the detection of LC3 (cat. no. 12741), Beclin-1 (cat. no. 3495), phosphorylated (p-)70S6K (Thr389; cat. no. 9234) and 70S6 (cat. no. 9202), cleaved poly (ADP-ribose) polymerase (PARP; cat. no. 5625) and PARP (cat. no. 9542) were procured from Cell Signaling Technology Inc. and the antibody for β-actin (cat. no. sc-69879) was sourced from Santa Cruz Biotechnology, Inc. Additional items included mouse Anti-β-Actin (cat. no. HC201; TransGen Biotech Co., Ltd.), rabbit Anti ATG5 (cat. no. ab108327, Abcam), BCA Protein Quantification Kit, TRIzol® reagent (Invitrogen; Thermo Fisher Scientific, Inc.), Ultrapure RNA/miRNA Extraction Kit (Thermo Fisher Scientific, Inc.), CCK-8 Assay Cell Proliferation Detection Kit (cat. no. KGA317;Nanjing KGI Biological Technology Development Co., Ltd.), ECL Ultra-sensitive Luminescent Solution (Thermo Fisher Scientific, Inc.) and Annexin V-FITC/PI Apoptosis Detection Kit (cat. no. C1062S; Beyotime Institute of Biotechnology).

Cell culture. HepG2 or Huh7 cells, free of mycoplasma, were purchased from Guangzhou Kinlogix Biotech Co., Ltd., which were genotypically verified using short tandem repeat analysis profiling by the vendor. The cells were cultured in 25 cm^2 flasks using Dulbecco's modified Eagle's medium (Invitrogen; Thermo Fisher Scientific, Inc.) supplemented with 10% (v/v) fetal bovine serum (FBS; Invitrogen; Thermo Fisher Scientific, Inc.), 100 IU/ml penicillin (Invitrogen; Thermo Fisher Scientific, Inc.) and 100 μg/ml streptomycin (Invitrogen; Thermo Fisher Scientific, Inc.). The cells were maintained at 37˚C in a humidified incubator with 5% CO_2, undergoing a 1:2 splitting every 2 to 3 days.

Small molecule compound libraries. A total of 3,271 small molecule compounds were sourced from the Prestwick Chemical Library containing 1,200 compounds, Tocriscreen plus (cat. no. 5840; Tocris Bioscience) with 1,119 compounds and SelleckChem Bioactive Compound Library-I (cat. no. L1700; Selleck Chemicals) comprising 952 compounds. These compounds have been extensively used for screening due to their established biological and pharmacological properties, validated safety profiles and proven efficacy in (pre-)clinical trials.

High-throughput screening (HTS). The HepG2 and Huh7 cells were seeded into 384-well flat bottom microtiter plates (cat. no. 353962; Becton, Dickinson and Company), with 800 cells in 50 μl medium per well using Multidrop Combi Reagent Dispenser (Thermo Fisher Scientific, Inc.). In total 3,271 small molecules at the final concentration of 10 μM were separately transferred to the corresponding wells using an Echo555 dispenser (Labcyte; Beckman Coulter, Inc.). After 48 h incubation, cells were fixed by 4% paraformaldehyde solution at room temperature for 10 min, stained with Hoechst with a final concentration of 1 μg/ml for 15 min at room temperature and finally subjected to automated image acquisition and nuclei counting by Acumen Cellista Laser Scanning Imaging Cytometer (TTP Labtech, Ltd.). Hit compounds were selected based on the nuclei counting assay in both liver cancer lines. The number of liver cancer cells in each plate was visualized through heatmaps produced by built-in Cellista software version 1.0 (TTP Labtech, Ltd.). Darker shades denoted lower cell counts, while greener shades indicated higher cell counts.

Hit selection. In the screening, where each compound underwent a single measurement, the Z score was used for hit identification. This approach is suitable for screens lacking replicates, assuming a normal distribution of measured values for all compounds under test on each plate. To calculate the Z score, the standard deviation of each plate was estimated from the median absolute deviation of the nuclei number across all tested 384-well plates. The Z score was calculated using the population mean and population standard deviation as $Z=(x-\mu)/\sigma$, where x represents the measurement of each compound under test, μ denotes the mean of the population and σ signifies the standard deviation of the population. A Z score threshold of -1.5 was chosen to robustly pinpoint liver cancer-killing compounds, mitigating false positives. This threshold corresponds to a 99.93% probability for a compound identified as a true hit.

Drug treatment. PD161570 was dissolved in DMSO to prepare a stock concentration of 10 mM and CQ was dissolved in DMSO to prepare a stock concentration of 20 mM; stock solutions were aliquoted and stored at -20˚C. The liver cancer cells were seeded in 6-well plates at a density of $2x10^5$ cells/well and were allowed to adhere overnight. Subsequently, the culture medium was replaced with fresh medium containing 10 μM PD161570 and 20 μM CQ, and the cells were incubated for 24 h at 37˚C in a humidified atmosphere containing 5% CO_2.

Cell Counting Kit (CCK-8) assay. Cells were cultured in 96-well plates and incubated for 24 h following their respective treatments. The medium was then replaced with fresh medium and 10 μl of CCK-8 reagent (cat. no. KGA317; Nanjing KeyGen Biotech Co., Ltd.) was added to each well. The plates were incubated at 37˚C for 2-4 h. Finally, absorbance at 450 nm was measured using a microplate reader (SuPerMax3100; Shanghai Flash Spectrum Biological Technology Co., Ltd.) for each well to assess cell viability.

Flow cytometry. Cells from each treatment group, totaling $1x10^6$, were harvested and centrifuged at 300 x g and room temperature for 3 min. The cells were washed twice with PBS and resuspended in 300 μl of pre-cooled 1XAnnexin V-FITC conjugate using the Annexin V-FITC/PI Apoptosis Detection Kit (cat. no. C1065S; Beyotime Institute of Biotechnology). Next, 5 μl of Annexin V-FITC and 10 μl of propidium iodide (PI) were added per well and after gentle mixing, the cells were incubated with the reagents at room temperature in darkness for 10 min and immediately analyzed by flow cytometry (FACSAria; BD Biosciences). The data were analyzed using BD FACSDiva™ Software v8.0 (BD Biosciences). The total apoptotic rate was calculated as the sum of the percentages of early (Annexin V-positive/PI-negative cells) and late (Annexin V-positive/PI-positive cells) apoptotic cells.

Cell transfection. When HepG2 cell density reached ~70%, indicating readiness for transfection, cells were cultured in serum-free medium. For transfection preparation, two sterilized Eppendorf tubes were used, with 125 μl of Opti-MEM (Invitrogen; Thermo Fisher Scientific, Inc.) added to each. Then, 5 μl of Lipofectamine® 3000 (Invitrogen; Thermo Fisher Scientific, Inc.) was added to one tube and 10 μl Atg5 siRNA or negative control siRNA at a concentration of 50 nM (previously dissolved in DEPC water at 100 μl/OD) to the other. The contents of both tubes were mixed thoroughly and incubated at 4˚C for 5 min. The contents of the two tubes were then combined, mixed again and incubated at room temperature for 15 min. The resulting mixture was added dropwise to the corresponding wells of a six-well plate and the cells were returned to the incubator. After 4 h, 1 ml of complete medium containing 20% serum was added to each well. Subsequent experiments were continued after an additional 48 h of incubation. The following sequences were synthesized by General Biology (Anhui) Co Ltd.: *ATG5* siRNA, 5'-GGAAUAUCC UGCAGAAGAAdTdT-3' (sense) and 5'-UUCUUCUGCAGG AUAUUCCdTdT-3' (antisense); negative control siRNA, sense: 5'-UUCUCCGAACGUGUCACGUdTdT-3' (sense) and 5'-ACGUGACACGUUCGGAGAAdTdT-3' (antisense).

Reverse transcription-quantitative PCR (RT-qPCR). When the cell density reached 75-85%, total cellular RNA was extracted using TRIzol™ Plus RNA Purification Kit (cat. no. 12183555; Invitrogen; Thermo Fisher Scientific, Inc.) according to the manufacturer's protocols. The concentration and purity of mRNA were assessed (OD260/OD280 ratio) using a UV-visible spectrophotometer (NP80 NanoPhotometer; Implen GmbH). For RT of RNA into cDNA, the High Capacity cDNA RT Kit (cat. no. 4368814; Applied Biosystems; Thermo Fisher Scientific, Inc.) was used according to the manufacturer's protocol. Briefly, after the removal of genomic DNA and determination of total RNA concentration, 1 pg-1 μg total RNA and 4 μl 4X gDNA wiper Mix were gently mixed in an RNase-free PCR tube with RNase-free ddH_2O to 16-μl total volume. RT was achieved via incubation at 42˚C for 30 min. Subsequently, the mRNA levels were quantified using SYBR Green PCR master mix (Shanghai Yeasen Biotechnology Co., Ltd.) on a fluorescence PCR instrument (CFX Connect; Bio-Rad Laboratories, Inc.). The data were analyzed with the $2^{-\Delta\Delta Cq}$ method according to the manufacturer's instructions (9). The data were normalized to the housekeeping gene *ACTB*. Changes in gene expression were illustrated as a fold increase/decrease. The experiments were repeated three times. Human primers used in the present study were as follows: 5'-CACAAGCAACTCTGGATGGGA-3' (Forward) and 5'-CAGCCACAGGACGAAACAG-3' (reverse) for *ATG5*; 5'-TCGCCAATTTTCAGGAGTTAGC-3' (forward) and 5'-CGCAAGAAACGGCAGAGATG-3' (reverse) for *DRAM1*; 5'-TGGCACCCAGCACAATGAA-3' (forward) and 5'-CTA AGTCATAGTCCGCCTAGAAGCA-3' (reverse) for *ACTB*.

Western blotting. Cells were pelleted by centrifugation at 300 x g for 10 min at room temperature and lysed in buffer (cat. no. P0013B; Beyotime Institute of Biotechnology) containing 50 mM Tris-HCl (pH 7.4), 0.15 M NaCl and 1% Triton X-100 for 30 min on ice. The lysates were then centrifuged at 15,000 g and 4˚C for 15 min. The BCA Protein Assay Kit (Thermo Fisher Scientific, Inc.) was used for the colorimetric detection and quantification of total proteins. Proteins obtained from cell lysates (20-40 μg protein/lane) were then separated by SDS-PAGE on 10 or 15% gels and transferred onto PVDF membranes. After blocking with 5% non-fat milk at room temperature for 2 h, the membranes were incubated with primary antibodies overnight at 4˚C and with secondary antibodies for 2 h at room temperature. The dilution for primary antibodies against p62, LC3, Beclin-1, ATG5, anti-p-70S6K (Thr389) and cleaved-PARP was 1:1,000, while 1:2,000 for β-actin. The dilution for HRP-linked secondary antibodies (cat. no. 7074; CST) was 1:5,000. Development was performed using Super Signal West Duration Substrate or Femto Stable Peroxide Solution (Thermo Scientific, Inc.) and images were captured with a Bio-Rad CCD camera. Results were analyzed using Image Lab Software version 5.2.1 (Bio-Rad Laboratories, Inc.).

RNA sequencing. Cellular RNA was extracted after different treatments using TRIzol Plus RNA Purification Kit. mRNA quantification for library preparation was conducted using Hieff NGS™ MaxUp Dual-mode mRNA Library Prep Kit for Illumina® (cat. no. 12301ES96; Shanghai Yeasen Biotechnology Co., Ltd.) and Hieff NGS® DNASelection Beads (cat. no. 12601ES56; Shanghai Yeasen Biotechnology Co., Ltd.). The procedures included mRNA purification, fragmentation, synthesis and purification of double-stranded cDNA, followed by the addition of dA tails and adapter ligation. The quality and concentration of the processed samples were verified using 2100 Bioanalyzer (Agilent Technologies, Inc.) and Qubit dsDNA HS Assay (cat. no. Q32851; Invitrogen; Thermo Fisher Scientific, Inc.) with the Qubit 2.0 Fluorometer (cat. no. Q32866; Invitrogen; Thermo Fisher Scientific, Inc.), respectively. Following purification, the double-stranded cDNAs were tagmented, amplified, quantified and pooled at an equal concentration of 2 nM. The quality and concentration of libraries were validated using 2100 Bioanalyzer (Agilent Technologies, Inc.) and qPCR (Kapa Library Quantification Kit; cat. no. KK4854; Roche Diagnostics), respectively. Subsequently, the libraries were sequenced on a NovaSeq 6000 sequencer (Illumina, Inc.) using the NovaSeq 6000 S1 Reagent Kit (cat. no. 20012860; Illumina, Inc.) with paired-end sequencing (150 bp read length). Raw sequencing data were processed using FastQC v0.12.0 (https://www.bioinformatics.babraham.ac.uk/projects/fastqc/) for quality control. Gene Ontology (GO) enrichment analysis was conducted using TopGO v2.58.0 (https://bioconductor.org/packages/release/bioc/html/topGO.html) to generate significant GO-directed graphs. Additionally, Kyoto Encyclopedia of Genes and Genomes (KEGG) pathway enrichment analysis was performed using clusterProfiler v4.15.1 (https://bioconductor.org/packages/devel/bioc/html/clusterProfiler.html). RNA sequencing and subsequent analyses were carried out by Sangon Biotech Co., Ltd. following standardized protocols.

Statistical analysis. All cellular experiments were conducted with a minimum of three biological replicates to ensure reliability. Data are expressed as mean ± SD and the specific number of experiments is detailed in the figure legends. Statistical analysis was performed using SPSS 23 statistics

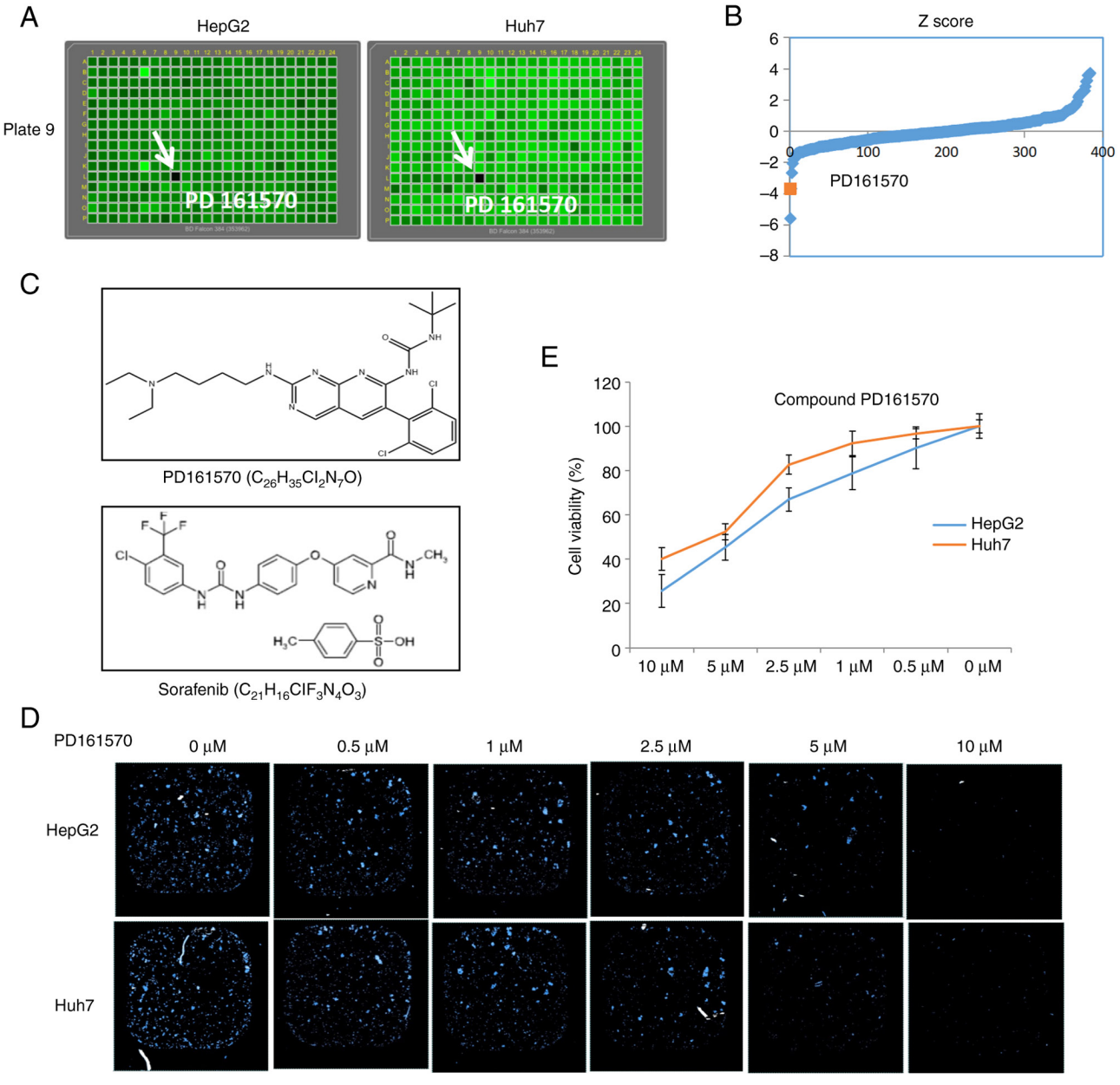

Figure 1. A high throughput chemical compound screen identified PD161570 as inducing cell death in a dose-dependent manner in liver cancer cells. (A) The liver cancer cell number readouts of each plate were illustrated using heatmaps generated by Cellista software, where darker shades indicated fewer cells, and greener shades represented more cells. PD161570 (highlighted by the arrows) was identified from plate 9 as a potential agent capable of inducing cell death in both HepG2 and Huh7 cell lines. (B) The selection of potential hits from each screening plate was based on setting the cutoff at Z score <1.5, with PD161570 exhibiting a Z score well below this threshold. (C) The structure and formula of PD161570 and Sorafenib. (D) The killing effect of PD161570 across different concentrations (0-10 μM) on HepG2 and Huh7 cells in a 384-well plate was visualized under a magnification of x4 through a nucleus counting assay after 48 h incubation period. (E) HepG2 and Huh7 cell lines were treated with varying concentrations of PD161570 to assess the cell-killing effects using a CCK-8 assay. The experiment was performed in triplicates, with the data represented as mean ± SD.

software (IBM Corp.). The t-test (two-tailed and unpaired) was used to evaluate association with parametric variables between two independent samples, and one-way ANOVA with Tukey's post hoc test was employed to account for multiple comparisons. P<0.05 was considered to indicate a statistically significant difference.

Results

Identification of PD161570 as an inhibitor of liver cancer cell proliferation. The poorly differentiated liver cancer cell lines, HepG2 and Huh7, were used to screen three small molecule libraries (Prestwick, Tocriscreen and SelleckChem Bioactive Compound Library-I), comprising 3,271 chemical compounds. Initial screening identified PD161570 as capable of killing both liver cancer cell lines (Fig. 1A). Screening was evaluated by calculating Z-scores for each plate to identify potential hits. As indicated in Fig. 1B, the Z-score of PD161570 fell below -1.5, suggesting its potential as a potent compound to attenuate liver cancer proliferation. The molecular structure and formula of PD161570 was shown in Fig. 1C as comparison with sorafenib, a TKI as first-line treatment for liver cancer.

Following its identification, PD161570 was subjected to a dose-response analysis at various concentrations (0-10 μM). Results from nuclei counting (Fig. 1D) and the CCK-8 assay (Fig. 1E) demonstrated a dose-dependent inhibition of liver cancer cell viability over 48 h. Notably, the inhibitory effect was more pronounced in HepG2 cells than in Huh7 cells.

PD161570 induces ATG5-dependent and mTOR-independent autophagy in hepatoma cells. Numerous studies have underscored the vital role of autophagy in liver cancer pathogenesis (10-13). Microtubule-associated protein LC3, a mammalian homolog of ATG8, is frequently used as a specific marker for autophagy activity (14). LC3 is characterized by two bands (LC3-I and LC3-II) on immunoblots, with LC3-II being preferred for its increased sensitivity in detecting autophagy in mammalian cells (14). Conversely, p62, which directly interacts with LC3, is essential in autophagosome formation and autophagic degradation (15,16). To assess autophagy induction by PD161570 in HepG2 and Huh7 cells, LC3 and p62 levels were analyzed. An increase in LC3-II levels was noted in a concentration-dependent manner in cells treated with PD161570 (Fig. 2A), while p62 expression significantly decreased at concentrations of 5 and 10 μM.

ATGs constitute a conserved gene set vital for autophagy mechanisms (17). In hepatoma cells treated with PD161570, ATG5 expression was significantly elevated at both 5 and 10 μM doses compared with untreated cells, whereas Beclin-1 levels remained stable (Fig. 2A). To explore the association between PD161570's effects and autophagic flux, cells were co-treated with PD161570 and CQ, an inhibitor of autophagosome degradation commonly used to assess autophagic flux. Co-treatment with PD161570 (10 μM) and CQ (20 μM) led to a pronounced increase in LC3-II levels (Figs. 2B and S1), indicating enhanced autophagic flux by PD161570 in HepG2 and Huh7 cells. Further investigation revealed that PD161570-induced autophagy was modulated independently of mTOR kinase, a critical autophagy regulator. Significant upregulation of p70S6K phosphorylation at Thr389, indicative of mTOR activity (18), was observed in PD161570-treated HepG2 and Huh7 cells compared with untreated cells (Fig. 2B), suggesting that PD161570 induces autophagy independently of mTOR signaling. These findings suggested that PD161570 triggers ATG5-dependent and mTOR-independent autophagy in both liver cancer cell lines.

Autophagy inhibition enhances PD161570-induced cell death and suppresses cell proliferation. The complex relationship between autophagy and apoptosis has been established as a key factor in hepatic cell death and the progression of liver diseases, supported by both pre-clinical models and clinical trials. The Annexin V-FITC/PI assay was used to detect changes in cell death, categorizing cells as viable (Annexin V-/PI-), early apoptotic (Annexin V+/PI-) and late apoptotic or necrotic (Annexin V+/PI+). To explore the effects of PD161570 on apoptosis under autophagy inhibition, co-treatment of PD161570 (10 μM) with CQ (20 μM) was found to enhance apoptosis and necrosis in both HepG2 and Huh7 cell lines, as indicated by the Annexin V/PI assay (Fig. 2C). Furthermore, the expression of cleaved PARP, a marker of apoptosis, was increased in the combination group compared with the groups treated singly with PD161570 or CQ (Figs. 2B and S1). Additionally, cell viability was significantly reduced by the combined treatment of PD161570 and CQ for 48 h, as shown by the CCK-8 assay results in Fig. 2D.

RNA-seq analysis of cells treated with PD161570 under autophagy inhibition. To explore the effect of PD161570 under conditions of autophagy inhibition via ATG5 silencing in HepG2 cells, gene expression profiling was conducted using RNA-seq. A comparison was made between cells treated with ATG5 siRNA and PD161570 and those treated only with ATG5 siRNA. Fig. 3A shows a substantial decrease in mRNA expression following ATG siRNA treatment, confirming the efficacy of the interference. Replications were performed three times for each experimental group. Differential gene expression analysis utilized thresholds of a q-value <0.05 and a fold change >2, identifying 1,121 differentially expressed genes. Among these, 613 genes were upregulated and 508 were downregulated, as shown in the differential expression scatter plot (Fig. 3B). Table I displays RNA-seq results, highlighting 15 genes with significant expression disparities (fold change >10). Among these genes, SAPCD1 was the most significantly downregulated, while VPREB3 was the most significantly upregulated. The genes listed in Table II, with fold changes >2, include those associated with apoptosis. Notable genes are HRK, CTSS, BIRC3, BBC3, DDIT3 and GADD45B indicating a significant role of apoptosis under autophagy deprivation.

DNA Damage Regulated Autophagy Modulator 1 (DRAM1) is a lysosomal membrane protein crucial for autophagy induction. Notably, DRAM1 is also a TP53 target gene known to modulate both autophagy and apoptosis, suggesting its dual role in influencing these processes. As the only upregulated autophagy-relevant gene, DRAM1 was identified from the RNA-seq analysis with a fold change of 1.4 in the present study, which was confirmed by the subsequent qPCR validation. Comparative analysis showed a significant increase in DRAM1 mRNA expression following transfection with ATG5 siRNA plus PD161570 treatment compared with ATG5 siRNA alone ($P<0.005$; Fig. 3C). Additionally, Annexin V/PI analysis was used to assess apoptotic responses in cells treated with PD161570 in combination with ATG5 siRNA. Results indicated a notable increase in apoptosis levels when 10 μM PD161570 was added to ATG5 siRNA-transfected cells compared with the ATG5 siRNA group (Fig. 3D and E), along with a significant decrease in cell proliferation (Fig. 3F). In summary, DRAM1 exhibited an increase rather than a decrease under conditions of autophagy inhibition, implying its potential role as a pro-apoptotic factor in response to PD161570 treatment and positioning it as a pivotal target for regulating both autophagy and apoptosis.

GO enrichment and KEGG pathway analyses of differentially expressed genes. GO provides a standardized framework for categorizing gene functions, offering an updated vocabulary to describe the properties of genes and their products comprehensively. Analysis presented in Fig. 4A showed significant changes in genes associated with the cellular response to stimulus, including those linked to apoptotic processes, apoptotic signaling

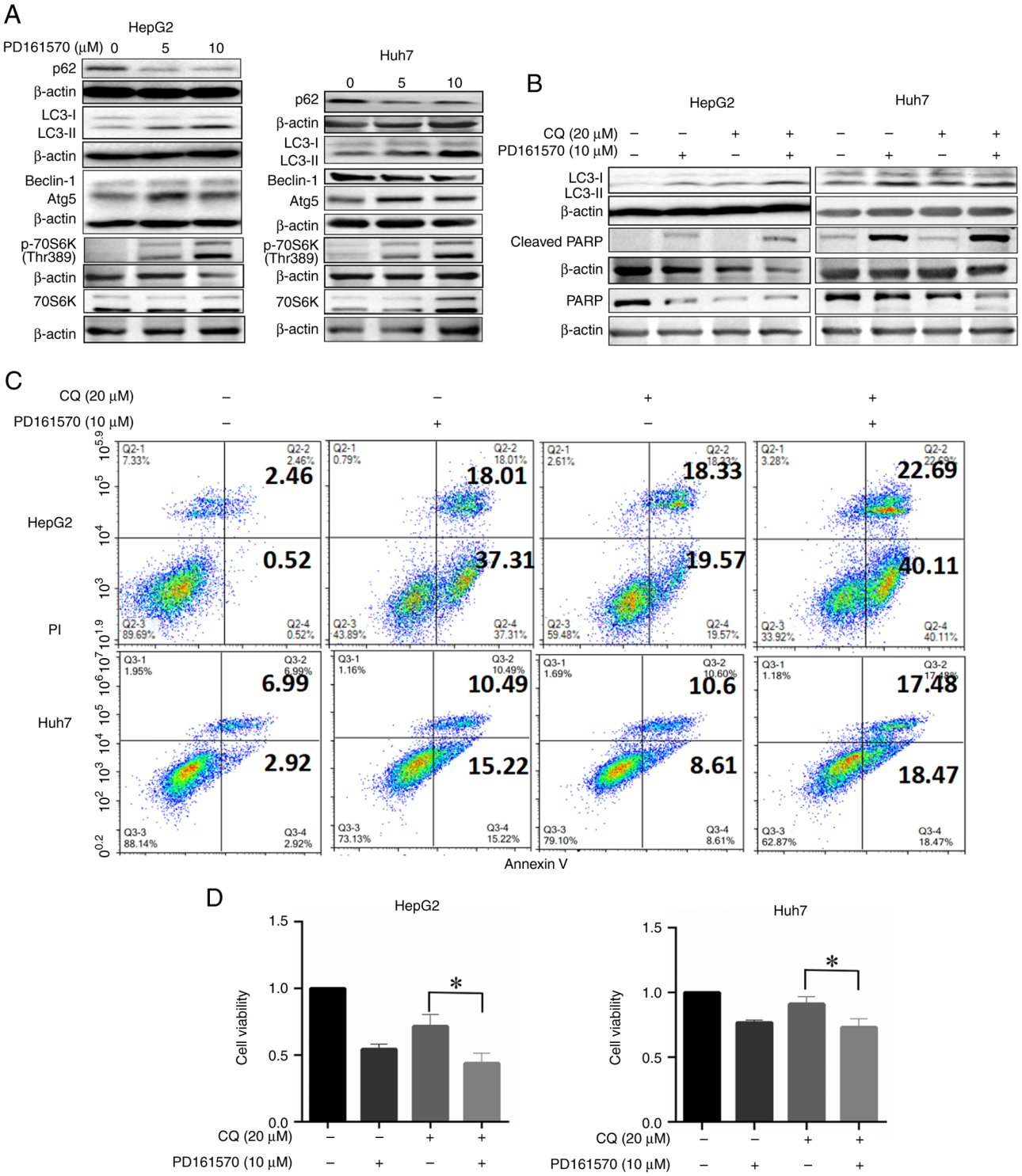

Figure 2. Treatment with PD161570 in HepG2 and Huh7 cells induces autophagy, while its combination with CQ enhances apoptosis. (A) Cell lysates, untreated and treated with various concentrations of PD161570 for 24 h, were analyzed by immunoblotting using antibodies against LC3, p62, ATG5, Beclin-1, 70S6k and 70S6K (Thr389). (B) Cell lysates, untreated and treated with PD161570 plus CQ for 24 h, were subjected to immunoblotting with antibodies against LC3, PARP and cleaved PARP. β-actin served as a loading control. Representative blots from three independent experiments are shown. (C) Apoptosis was assessed through Annexin V/PI analysis of HepG2 (top panel) and Huh7 (bottom panel) cells treated with PD161570 and/or CQ. (D) Cell viability, presented as relative to the control, was measured using a CCK-8 assay in HepG2 (top panel) and Huh7 (bottom panel) cells following treatment with PD161570 and/or CQ. Cell viability was presented as the mean ± SEM from three independent experiments, indicating significant differences between CQ treatment and combined treatment with PD161570 and CQ (*P<0.05). CQ, chloroquine; ATG5, autophagy-related gene 5; PARP, poly (ADP-ribose) polymerase.

pathways, cell death and cell differentiation, highlighting the critical roles of apoptosis-related genes under conditions of autophagy deprivation following PD161570 treatment. The KEGG integrates genomic, chemical and systemic functional information to provide insights into biological systems. KEGG analysis identified significant differences in pathways such as rat sarcoma (RAS), PI3K-Akt, MAPK, Forkhead box O (FOXO), Hippo and apoptosis. Notably, the MAPK signaling pathway

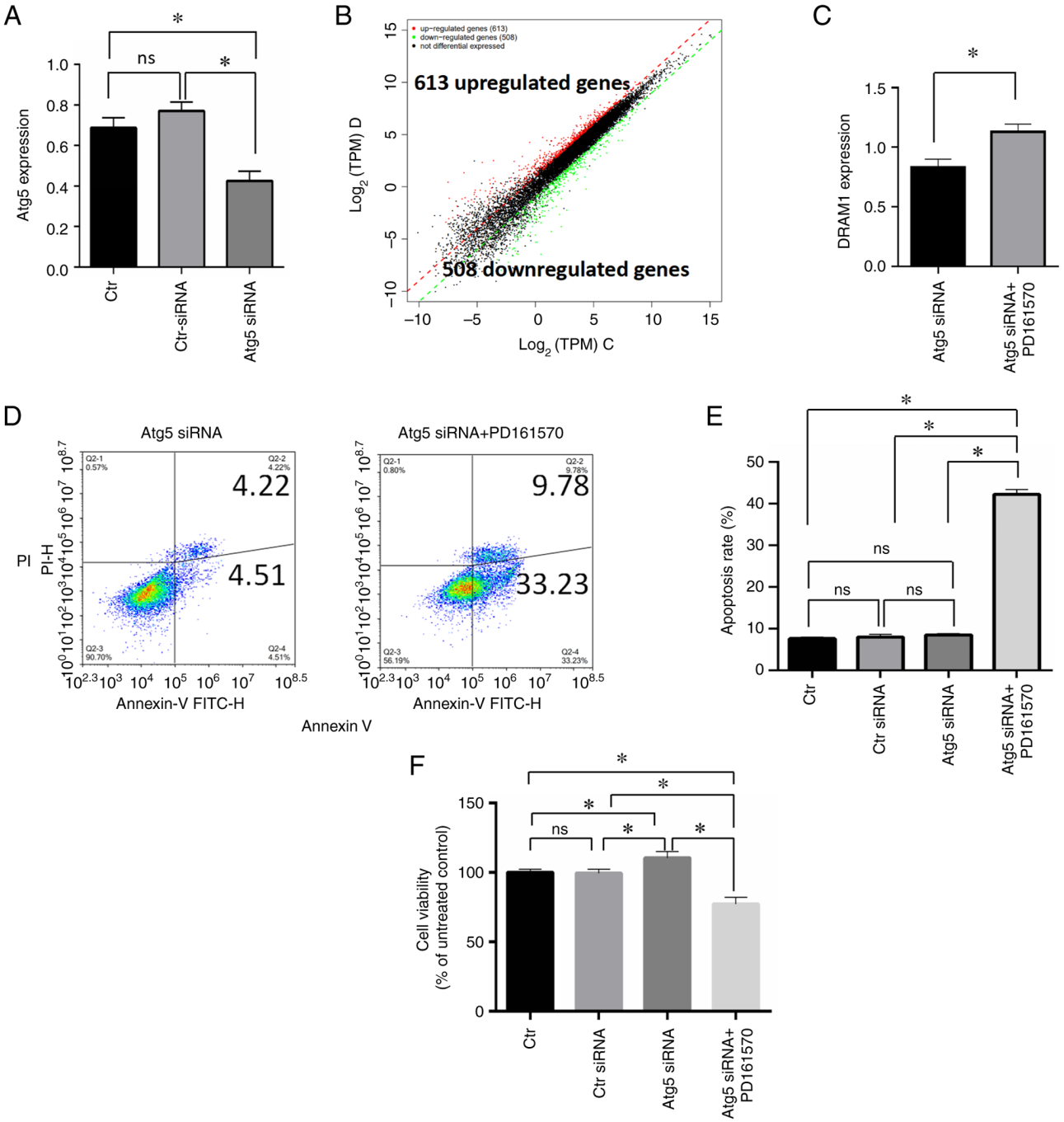

Figure 3. RNA-seq analysis to elucidate the underlying mechanism of PD161570. (A) RNA analysis validated ATG5 inhibition by ATG5 siRNA in HepG2 cells. (B) A differential expression scatter plot displayed log2 of TPM values of two sample sets, with red denoting upregulated genes, green indicating downregulated genes and black representing non-differentially expressed genes. (C) Immunoblotting analysis compared DRAM1 expression levels between ATG5 siRNA-transfected cells alone and those combined with 10 μM PD161570. (D) Annexin V/PI analysis assessed apoptosis levels between ATG5 siRNA-transfected cells alone and in combination with 10 μM PD161570. (E) Triplicate Annexin V/PI analysis of apoptotic cells between ATG5 siRNA-transfected cells alone and in combination with 10 μM PD161570 were represented as mean ± SD. Untreated cells and control siRNA-transfected cells served as loading controls. (F) Data from CCk-8 analysis of viable cells between ATG5 siRNA-transfected cells alone and in combination with 10 μM PD161570, performed in triplicates, is depicted as mean ± SD. *P<0.05. Untreated cells and control siRNA-transfected cells were included as loading controls. RNA-seq, RNA sequencing; ATG5, autophagy-related gene 5; si, small interfering; TPM, transcript per million; DRAM1, Damage Regulated Autophagy Modulator 1; Ctr, control.

was the most significantly altered (P=4.13x10^{-6}), followed by the apoptosis pathway (P=0.0006), as depicted in Fig. 4B.

Discussion

The present study focused on the mechanisms associated with TKIs, the primary targeted drugs for liver cancer. An automated and simple HTS assay was developed to rapidly screen small molecules, including PD161570 and mitoxantrone (19), which induce specific cell death in liver cancer cells. PD161570, identified as a novel TKI and fibroblast growth factor 1 receptor inhibitor (20,21), has limited information available about its mechanism of action. Although global research on this topic is minimal, previous literature has suggested that PD161570

Table I. Changes in gene expression (Fold change >12) induced by 10 μM PD161570 in HepG2 cells.

Log2FC	Gene name	Gene description
12.81	VPREB3	V-set pre-B cell surrogate light chain 3
12.78	SLC24A5	Solute carrier family 24 member 5
12.09	GZMM	Granzyme M
12.02	WNT9B	Wnt family member 9B
11.89	DNAAF1	Dynein axonemal assembly factor 1
11.75	SLC35G5	Solute carrier family 35 member g5
11.46	ENO4	Enolase family member 4
11.17	TGFB2	Transforming growth factor beta 2
-12.41	MCCD1	Mitochondrial coiled-coil domain 1
-12.44	C11orf97	Chromosome 11 open reading frame 97
-12.50	HAO2	Hydroxyacid oxidase 2
-12.89	HLA-G	Major histocompatibility complex, class I, G
-12.99	DNASE1L3	Deoxyribonuclease 1 like 3
-13.15	TAGLN3	Transgelin 3
-15.91	SAPCD1	Suppressor APC domain containing 1

Table II. List of selected top differentially expressed genes involved in autophagy or apoptosis in HepG2 cells.

Log2FC	Gene name	Gene description	Function
4.13	HRK	Harakiri	Apoptosis
2.46	CTSS	Cathepsin S	Apoptosis
2.44	BIRC3	Baculoviral IAP repeat containing 3	Apoptosis
2.21	BBC3	BCL2 binding component 3	Apoptosis
2.05	DDIT3	DNA damage inducible transcript 3	Apoptosis
2.03	GADD45B	Growth arrest and DNA damage inducible beta	Apoptosis
1.40	DRAM1	DNA damage regulated autophagy modulator 1	Autophagy

inhibits FGF-1 receptor phosphorylation in human ovarian cancer cells and in insect cells overexpressing human FGF-1 receptors (22). Additionally, PD161570 has shown efficacy in inhibiting basic FGF-mediated angiogenesis and inducing cell death in acute myeloid leukemia cells (23), highlighting its potential anti-tumor properties. Despite these findings, there is scant information on the effects of PD161570 on liver cancer, necessitating further research into its effects in this area.

In the present study, a rapid and straightforward assay was employed to screen a small molecule library, identifying compounds that induce significant cell death in liver cancer cells. Results from nuclei counting and viability assays indicated that PD161570 inhibited the growth and proliferation of hepatic cancer cells. Observations also showed an upregulation of LC3-II levels and a downregulation of p62 in PD161570-treated hepatic cancer cells, suggesting that PD161570 induced autophagy. When PD161570 was combined with CQ, an increase in LC3-II expression was observed, indicating enhanced autophagic activity. These results highlighted the robust autophagic flux prompted by PD161570, covering processes from induction to degradation. In the present study, elevated levels of the autophagy core protein ATG5 were detected in PD161570-treated liver cancer cells, suggesting the potential induction of ATG5-mediated autophagy by PD161570. A previous study identified mTOR as a critical sensor of cellular nutrient status, with its inhibition triggering autophagy under energy deprivation conditions (24). Notably, the present study indicated that PD161570 stimulated autophagy through an mTOR-independent pathway. This is consistent with existing research showing that certain small molecules, such as intracellular inositol or inositol 1,4,5-trisphosphate, can activate mTOR-independent autophagy *in vitro* (25,26). In conclusion, PD161570 induces autophagy by modulating autophagy-related genes, including ATG5, LC3-II and p62.

Cell death includes various mechanisms, such as apoptosis, necrosis and autophagic death (27,28). Among these, autophagy, necrosis and apoptosis are critical in anti-tumor therapy (29). Antitumor drugs often induce cell death, leading to the inhibition of cell growth and proliferation (30,31). There is growing evidence that autophagy and apoptosis interact in diverse ways; either antagonizing, assisting, or influencing each other to determine cellular fate (32). Studies have elucidated the complex pathways through which autophagy and apoptosis interact (32,33). In the present study, inhibition of autophagy by CQ demonstrated that PD161570 facilitated necrotic and apoptotic cell death, thereby

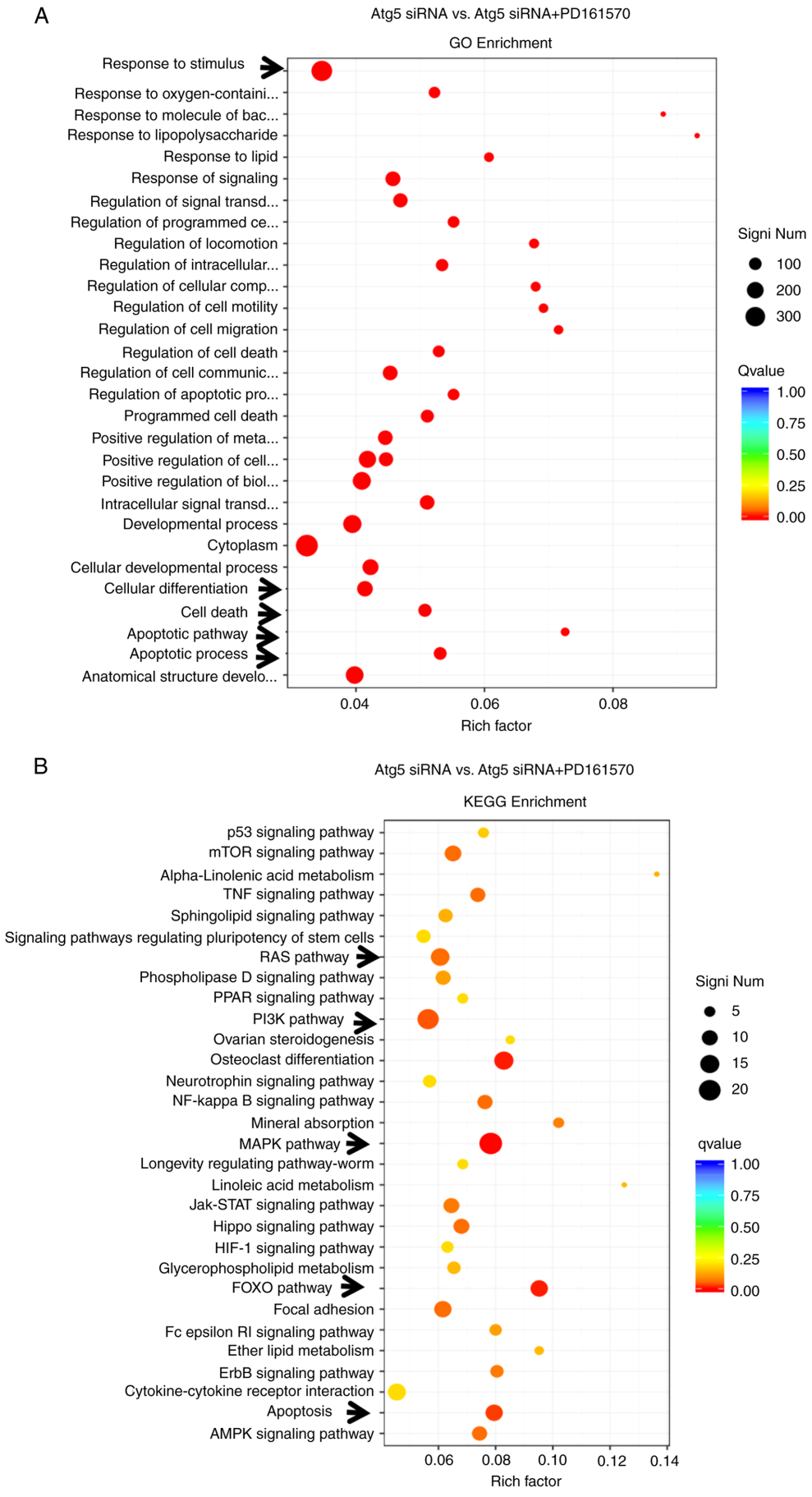

Figure 4. (A) GO and (B) KEGG analyses utilizing the upregulated genes from treatment with both ATG5 siRNA-transfection and PD161570, in comparison with only ATG5 siRNA-transfection. GO, Gene Ontology; KEGG, Kyoto Encyclopedia of Genes and Genomes; ATG5, autophagy-related gene 5; si, small interfering.

inhibiting the proliferation and growth of hepatic cancer cells. These findings suggested that suppressing autophagy sensitized hepatic cancer cells to PD161570 treatment. Consequently, it was concluded that PD161570-induced autophagy, apoptosis and necrosis collectively contributed to the death of hepatic cancer cells. In recent years, lysosomal cell death has emerged as a form of programmed cell death, alongside other processes such as pyroptosis, necroptosis and NETosis, which have been described in the literature (34). Currently, the authors have not explored other forms of cell death. However, in upcoming experiments for a new project, it is intended to investigate ferroptosis, a recently identified type of cell death that is associated with autophagy.

RNA sequencing technology was further utilized to investigate the mechanism underlying PD161570-mediated cell death in the context of autophagy inhibition via ATG5 knockdown. A total of 1,121 differentially expressed genes were identified from the combined treatment of PD161570 and ATG5 knockdown compared with the group with only ATG5 knockdown; 613 genes were upregulated, and 508 genes downregulated. Notably, among these genes, DRAM1 emerged as a key player in autophagy modulation. DRAM1, characterized by six membrane-spanning regions and predominantly located on the lysosomal membrane, functions as a TP53 target gene regulating both autophagy and apoptosis (35-37). It is hypothesized that DRAM1 may play a pivotal role in mediating PD161570-induced apoptosis and autophagy in hepatic cancer cells. The precise contribution of DRAM1 to liver cancer cell autophagy and apoptosis and the underlying mechanisms remain to be elucidated. It has been previously reported that DRAM1 knockdown by specific siRNA abrogated cell autophagy in HepG2 cells, which may be reversed by rapamycin treatment (38). The present study demonstrated that PD161570 induced ATG5-dependent autophagy and promoted autophagic flux in HepG2 cells. Notably, DRAM1 expression was found to increase rather than decrease following ATG5 knockdown using specific siRNAs. This increase in DRAM1 expression was associated with autophagy inhibition and enhanced apoptosis. The findings suggested that while DRAM1 may not directly participate in PD161570-induced autophagy, it could potentially be involved in the apoptosis triggered by PD161570. Under conditions of autophagy inhibition through ATG5 silencing, DRAM1 could potentially induce apoptosis, similar to findings in an experimental rat model where DRAM1 interacted with Atg7, rather than ATG5 (39). ATG5 may be a key crosstalk of autophagy and apoptosis in PD161570-treated liver cancer cells, though further experimental validation is required to confirm this hypothesis.

GO enrichment and KEGG pathway analyses revealed significant enrichment of genes associated with the apoptotic cell death response, suggesting that PD161570 may facilitate cell death via the apoptotic signaling pathway in the absence of autophagy. HRK, an apoptosis activator known as Harakiri, modulates apoptosis by interfering with anti-apoptotic Bcl-2 and Bcl-xL proteins (40,41). The role of HRK in tumors remains unclear, with limited evidence showing its downregulation in tumors contexts (42). Additionally, TGF-β2, a highly differentially expressed gene in the MAPK signaling pathway, was identified as participating in PD161570-induced apoptosis under autophagy inhibition. Beyond its role in inducing apoptosis, TGF-β2 may also function in breast cancer development, acting as a tumor suppressor in primary tumor initiation and a promoter in later stages (43). However, the roles of HRK and TGF-β2 in PD161570-induced apoptosis alongside autophagy inhibition requires further investigation.

In conclusion, the present study provided the first documentation of the potential of PD161570 as a liver cancer therapeutic agent, highlighting its interactions with autophagy and apoptosis pathways. PD161570 triggers ATG5-dependent and mTOR-independent autophagy in hepatic cancer cells and promotes apoptosis when autophagy is inhibited. These findings underscore the need for further research into drug development for hepatocellular carcinoma treatment. However, the detailed molecular mechanisms linking PD161570 to these pathways remain to be fully elucidated.

Acknowledgements

The authors would like to thank Professor Jinping Li (Department of Medical Biochemistry and Microbiology, University of Uppsala, Sweden) for language refining and modification.

Funding

The present study was supported by the Jiangxi Provincial Youth Science Foundation (grant no. 20202ACBL216014), the Jiangxi Provincial Natural Science Foundation (grant no. 20232BAB206164), the Key Laboratory Project of Digestive Diseases in Jiangxi Province (grant no. 2024SSY06101) and Jiangxi Clinical Research Center for Gastroenterology (grant no. 20223BCG74011).

Availability of data and materials

The data generated in the present study may be requested from the corresponding author. The raw RNA sequencing data generated in the present study may be found in the Sequence Read Archive database under accession number PRJNA1187334 or at the following URL: https://www.ncbi.nlm.nih.gov/sra/PRJNA1187334.

Authors' contributions

BX designed the study, drafted and revised the manuscript, XH performed the experiments and collected data, JL performed the experiments and revised the manuscript and YZ performed the statistical analysis. XH and BX confirm the authenticity of all the raw data All authors read and approved the final version of the manuscript.

Ethics approval and consent to participate

Not applicable.

Patient consent for publication

Not applicable.

Competing interests

The authors declare that they have no competing interests.

References

1. Song P, Tang W, Tamura S, Hasegawa K, Sugawara Y, Dong J and Kokudo N: The management of hepatocellular carcinoma in Asia: a guideline combining quantitative and qualitative evaluation. Biosci Trends 4: 283-287, 2010.
2. Frenette C and Gish R: Targeted systemic therapies for hepatocellular carcinoma: Clinical perspectives, challenges and implications. World J Gastroenterol 18: 498-506, 2012.
3. Mandlik DS, Mandlik SK and Choudhary HB: Immunotherapy for hepatocellular carcinoma: Current status and future perspectives. World J Gastroenterol 29: 1054-1075, 2023.
4. Luo X, He X, Zhang X, Zhao X, Zhang Y, Shi Y and Hua S: Hepatocellular carcinoma: Signaling pathways, targeted therapy and immunotherapy. MedComm (2020) 5: e474, 2024.
5. Feng MY, Chan LL and Chan SL: Drug treatment for advanced hepatocellular carcinoma: First-line and beyond. Curr Oncol 29: 5489-5507, 2022.
6. Richards KN, Zweidler-McKay PA, Van Roy N, Speleman F, Trevino J, Zage PE and Hughes DP: Signaling of ERBB receptor tyrosine kinases promotes neuroblastoma growth in vitro and in vivo. Cancer 116: 3233-3243, 2010.
7. Hussain S, Mursal M, Verma G, Hasan SM and Khan MF: Targeting oncogenic kinases: Insights on FDA approved tyrosine kinase inhibitors. Eur J Pharmacol 970: 176484, 2024.
8. Rosenzweig SA: Acquired resistance to drugs targeting tyrosine kinases. Adv Cancer Res 138: 71-98, 2018.
9. Livak KJ and Schmittgen TD: Analysis of relative gene expression data using real-time quantitative PCR and the 2(-Delta Delta C(T)) Method. Methods 25: 402-408, 2001.
10. Hashemi M, Nadafzadeh N, Imani MH, Rajabi R, Ziaolhagh S, Bayanzadeh SD, Norouzi R, Rafiei R, Koohpar ZK, Raei B, *et al*: Targeting and regulation of autophagy in hepatocellular carcinoma: revisiting the molecular interactions and mechanisms for new therapy approaches. Cell Commun Signal 21: 32, 2023.
11. Chao X, Qian H, Wang S, Fulte S and Ding WX: Autophagy and liver cancer. Clin Mol Hepatol 26: 606-617, 2020.
12. Akkoc Y and Gozuacik D: Autophagy and liver cancer. Turk J Gastroenterol 29: 270-282, 2018.
13. Di Fazio P and Matrood S: Targeting autophagy in liver cancer. Transl Gastroenterol Hepatol 3: 39, 2018.
14. Tanida I, Minematsu-Ikeguchi N, Ueno T and Kominami E: Lysosomal turnover, but not a cellular level, of endogenous LC3 is a marker for autophagy. Autophagy 1: 84-91, 2005.
15. Pankiv S, Clausen TH, Lamark T, Brech A, Bruun JA, Outzen H, Øvervatn A, Bjørkøy G and Johansen T: p62/SQSTM1 binds directly to Atg8/LC3 to facilitate degradation of ubiquitinated protein aggregates by autophagy. J Biol Chem 282: 24131-24145, 2007.
16. Kabeya Y, Mizushima N, Ueno T, Yamamoto A, Kirisako T, Noda T, Kominami E, Ohsumi Y and Yoshimori T: LC3, a mammalian homologue of yeast Apg8p, is localized in autophagosome membranes after processing. EMBO J 19: 5720-5728, 2000.
17. Kabeya Y, Mizushima N, Yamamoto A, Oshitani-Okamoto S, Ohsumi Y and Yoshimori T: LC3, GABARAP and GATE16 localize to autophagosomal membrane depending on form-II formation. J Cell Sci 117: 2805-2812, 2004.
18. Pullen N and Thomas G: The modular phosphorylation and activation of p70s6k. FEBS Lett 410: 78-82, 1997.
19. Xie B, He X, Guo G, Zhang X, Li J, Liu J and Lin Y: High-throughput screening identified mitoxantrone to induce death of hepatocellular carcinoma cells with autophagy involvement. Biochem Biophys Res Commun 521: 232-237, 2020.
20. Horakova D, Cela P, Krejci P, Balek L, Moravcova Balkova S, Matalova E and Buchtova M: Effect of FGFR inhibitors on chicken limb development. Dev Growth Differ 56: 555-572, 2014.
21. Stevens DA, Harvey CB, Scott AJ, O'Shea PJ, Barnard JC, Williams AJ, Brady G, Samarut J, Chassande O and Williams GR: Thyroid hormone activates fibroblast growth factor receptor-1 in bone. Mol Endocrinol 17: 1751-1766, 2003.
22. Batley BL, Doherty AM, Hamby JM, Lu GH, Keller P, Dahring TK, Hwang O, Crickard K and Panek RL: Inhibition of FGF-1 receptor tyrosine kinase activity by PD 161570, a new protein-tyrosine kinase inhibitor. Life Sci 62: 143-150, 1998.
23. Biyanee A, Yusenko MV and Klempnauer KH: Src-Family protein kinase inhibitors suppress MYB activity in a p300-dependent manner. Cells 11: 1162, 2022.
24. Jaboin JJ, Shinohara ET, Moretti L, Yang ES, Kaminski JM and Lu B: The role of mTOR inhibition in augmenting radiation induced autophagy. Technol Cancer Res Treat 6: 443-447, 2007.
25. Rubinsztein DC, Gestwicki JE, Murphy LO and Klionsky DJ: Potential therapeutic applications of autophagy. Nat Rev Drug Discov 6: 304-312, 2007.
26. Botti J, Djavaheri-Mergny M, Pilatte Y and Codogno P: Autophagy signaling and the cogwheels of cancer. Autophagy 2: 67-73, 2006.
27. Repici M, Mariani J and Borsello T: Neuronal death and neuroprotection: A review. Methods Mol Biol 399: 1-14, 2007.
28. Yan L, Liu C, Zhai Z, Ren G and Qiu S: A review of research progress on the mechanisms of programmed nerve cell death. Altern Ther Health Med 30: 68-72, 2024.
29. Liu W, Jin W, Zhu S, Chen Y and Liu B: Targeting regulated cell death (RCD) with small-molecule compounds in cancer therapy: A revisited review of apoptosis, autophagy-dependent cell death and necroptosis. Drug Discov Today 27: 612-625, 2022.
30. Xie SB, He XX and Yao SK: Matrine-induced autophagy regulated by p53 through AMP-activated protein kinase in human hepatoma cells. Int J Oncol 47: 517-526, 2015.
31. Xie BS, He XX, Ai ZL and Yao SK: Involvement of β-catenin in matrine-induced autophagy and apoptosis in WB-F344 cells. Mol Med Rep 9: 2547-2553, 2014.
32. Xi H, Wang S, Wang B, Hong X, Liu X, Li M, Shen R and Dong Q: The role of interaction between autophagy and apoptosis in tumorigenesis (Review). Oncol Rep 48: 208, 2022.
33. D'Arcy MS: Cell death: A review of the major forms of apoptosis, necrosis and autophagy. Cell Biol Int 43: 582-592, 2019.
34. Park W, Wei S, Kim BS, Kim B, Bae SJ, Chae YC, Ryu D and Ha KT: Diversity and complexity of cell death: A historical review. Exp Mol Med 55: 1573-1594, 2023.
35. Liu K, Lou J, Wen T, Yin J, Xu B, Ding W, Wang A, Liu D, Zhang C, Chen D and Li N: Depending on the stage of hepatosteatosis, p53 causes apoptosis primarily through either DRAM-induced autophagy or BAX. Liver Int 33: 1566-1574, 2013.
36. Takahashi M, Kakudo Y, Takahashi S, Sakamoto Y, Kato S and Ishioka C: Overexpression of DRAM enhances p53-dependent apoptosis. Cancer Med 2: 1-10, 2013.
37. Crighton D, Wilkinson S and Ryan KM: DRAM links autophagy to p53 and programmed cell death. Autophagy 3: 72-74, 2007.
38. Chen C, Liang QY, Chen HK, Wu PF, Feng ZY, Ma XM, Wu HR and Zhou GQ: DRAM1 regulates the migration and invasion of hepatoblastoma cells via autophagy-EMT pathway. Oncol Lett 16: 2427-2433, 2018.
39. Wu X, Qin Y, Zhu X, Liu D, Chen F, Xu S, Zheng D, Zhou Y and Luo J: Increased expression of DRAM1 confers myocardial protection against ischemia via restoring autophagy flux. J Mol Cell Cardiol 124: 70-82, 2018.
40. Chang I, Majid S, Saini S, Zaman MS, Yamamura S, Chiyomaru T, Shahryari V, Fukuhara S, Deng G, Dahiya R and Tanaka Y: Hrk mediates 2-methoxyestradiol-induced mitochondrial apoptotic signaling in prostate cancer cells. Mol Cancer Ther 12: 1049-1059, 2013.
41. Kaya-Aksoy E, Cingoz A, Senbabaoglu F, Seker F, Sur-Erdem I, Kayabolen A, Lokumcu T, Sahin GN, Karahuseyinoglu S and Bagci-Onder T: The pro-apoptotic Bcl-2 family member Harakiri (HRK) induces cell death in glioblastoma multiforme. Cell Death Discov 5: 64, 2019.
42. Nakamura M, Shimada K and Konishi N: The role of HRK gene in human cancer. Oncogene 27 (Suppl 1): S105-S113, 2008.
43. Dave H, Trivedi S, Shah M and Shukla S: Transforming growth factor beta 2: A predictive marker for breast cancer. Indian J Exp Biol 49: 879-887, 2011.